

See discussions, stats, and author profiles for this publication at: <https://www.researchgate.net/publication/261601824>

# Hyphenating Atomic Force Microscopy

ARTICLE *in* ANALYTICAL CHEMISTRY · APRIL 2014

Impact Factor: 5.64 · DOI: 10.1021/ac5008128 · Source: PubMed

---

CITATIONS

4

---

READS

68

## 2 AUTHORS:



Alexander Eifert

Macherey-Nagel GmbH & Co. KG

9 PUBLICATIONS 23 CITATIONS

[SEE PROFILE](#)



Christine Kranz

Universität Ulm

130 PUBLICATIONS 2,449 CITATIONS

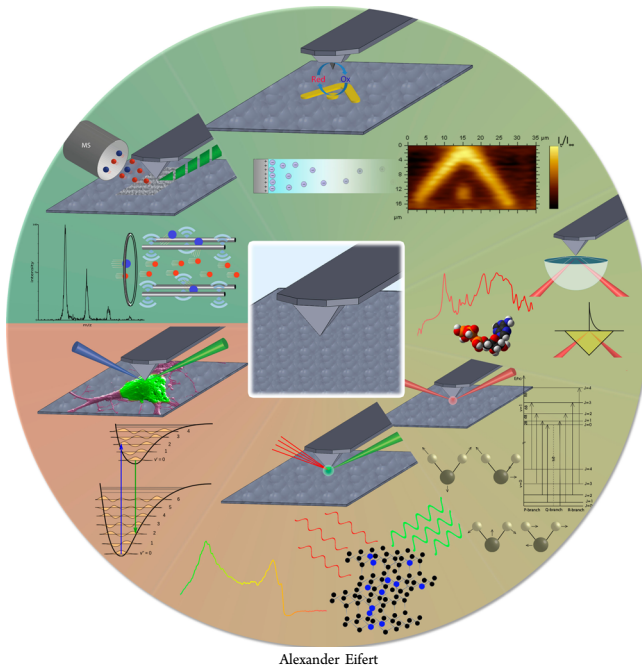
[SEE PROFILE](#)

# Hyphenating Atomic Force Microscopy

Atomic force microscopy can be readily combined with complementary instrumental techniques ranging from optical to mass-sensitive methods. This Feature highlights recent advances on hyphenated AFM technology, which enables localized studies and mapping of complementary information at surfaces and interfaces.

Alexander Eifert and Christine Kranz\*

Institute of Analytical and Bioanalytical Chemistry, University of Ulm, Albert-Einstein-Allee 11, 89081 Ulm, Germany



The term “*hyphenated*” is a readily established expression in analytical chemistry related to separation techniques and refers to the coupling of at least two individual instrumental strategies via a sample transfer line, e.g., a separation technique such as gas chromatography coupled to an advanced detection scheme such as mass spectrometry or IR spectroscopy. However, as already stated by T. Hirschfeld, “*hyphenation is beyond just coupling two techniques and refers to an automated single integrated unit, which is connected via a hardware interface.*”<sup>1</sup> To date, in scanning probe microscopy (SPM), the term “*hyphenated*” remains rarely used, as the combination of complementary techniques involving scanning probe microscopies does not necessarily reflect the combination of individual, i.e., stand-alone, analytical instruments. Moreover, in hyphenated SPM, the “*scanning probe*” frequently entails an advanced probe design integrating multi-functionality right into the tip. This Feature provides a general overview on current trends and approaches in *hyphenated* scanning force microscopy and highlights selected examples illustrating the utility of such strategies.

Atomic force microscopy (AFM) or more generally termed scanning force microscopy (SFM) was introduced by Binnig,

Quate, and Gerber in 1986<sup>2</sup> and has since become a true workhorse in many research fields, including routine characterization tasks in industrial settings due to its nondestructive high-resolution surface analysis capabilities. In AFM, the force between a sharp tip at the end of a cantilever with force constants ranging from 0.06 N/m (for soft sample imaging) to approximately 10 N/m and the sample leads to attractive or repulsive forces. These force interactions are typically detected with a laser beam, which is reflected from the end of the cantilever onto a split photodiode, thereby translating the force-induced deflection of the cantilever into a photo current. This photo current in turn is converted into an error signal that is used to regulate the distance between the tip and the sample surface. Scanning the sample thus results in a three-dimensional image of the surface topology and also provides information on the nanomechanical properties of the sample. Since the introduction of the first commercial AFM instrument by Digital Instruments in 1989, a multitude of imaging modes have been introduced enabling the characterization of physical sample properties such as elasticity, surface potentials, magnetism, electrostatic properties, work functions, magnetic properties, thermal changes, conductivity, and friction. The evident popularity of AFM is certainly related to the development of increasingly robust and easy-to-use instrumentation ranging from sophisticated AFM devices designed for ultrahigh vacuum (UHV) studies<sup>3</sup> to systems suitable for high-throughput routine surface characterization in industrial settings. Last but not least, AFM techniques are increasingly adopted in the life sciences and may, e.g., be located within an incubator suitable for imaging live biological systems at controlled temperature and CO<sub>2</sub> conditions in buffered solutions.<sup>4</sup> The possibility to measure intra- and/or intermolecular forces with pico-Newton precision at a single-molecule level is owed to the sophistication and fidelity of microfabricated AFM cantilevers, which are produced in batches with very high reproducibility. Typically, more than several hundreds of probes are microfabricated from a 4-in. silicon wafer substrate using conventional silicon processing techniques including lithography, wet-etching, etc.<sup>5</sup> Hence, cantilevers with different force constants, geometric features, and surface modifications such as specific coatings are readily available. Besides the versatility for analyzing physical surface parameters to the level of individual atoms, AFM is conversely lacking in chemical information, as it predominantly provides morphological information on the sample surface.

**Published:** April 10, 2014

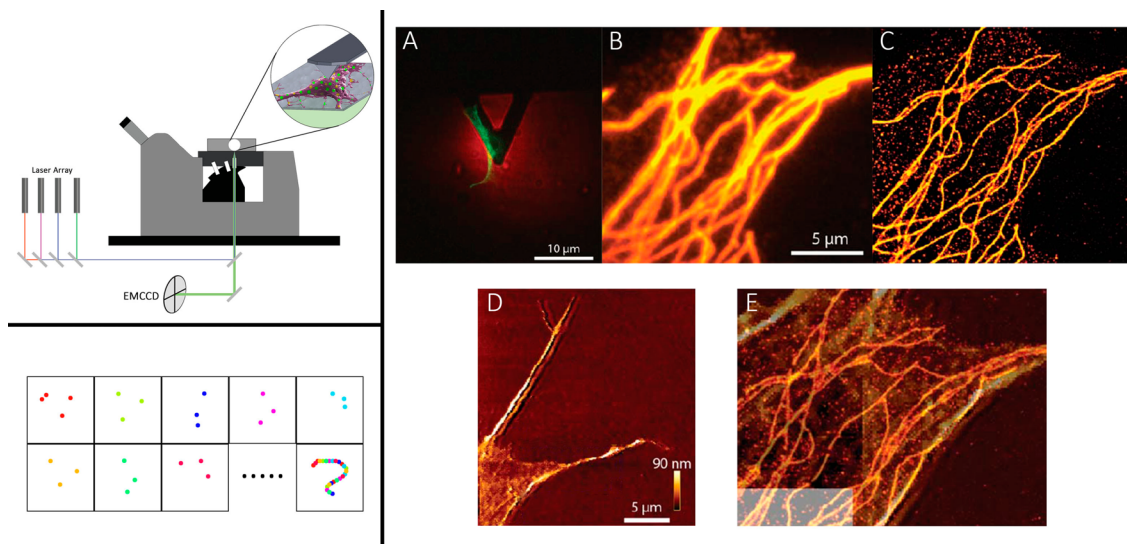


**Figure 1.** Schematic of a hybrid AFM-STORM instrument (left). (A) HeLa cell image overlaid with the image of the tip. Images B and C show the comparison of a wide field and STORM image of the same area, respectively. Part D represents a higher resolution AFM image providing the topology of single fibers. Part E shows the topological AFM image corresponding to the same region overlaid onto the STORM image. Reprinted with permission from ref 22. Copyright 2013 Wiley-VCH.

Consequently, a significant driving force behind hyphenating AFM with optical, electrochemical, and even mass-sensitive measurement techniques is from an analytical point of view the demand to provide complementary chemical information on the sample surface or surface processes. Complex analysis problems such as those encountered during biomedical studies, in heterogeneous catalysis, or when analyzing dynamic processes at solid/liquid and liquid/liquid interfaces, e.g., in corrosion sciences or energy-related research require the synergistic investigation of (electro)chemical, mechanical, and kinetic processes. In addition, these processes need to be understood at a molecular level and ideally with high temporal resolution, while the physical and chemical information is also correlated in the spatial domain. As demonstrated within the last decades, a promising approach to meet these requirements is combining atomic force microscopy with complementary analytical techniques toward hyphenated scanning probe platforms.

## ■ AFM COMBINED WITH OPTICAL MICROSCOPY

In instrumental analytical chemistry, almost the entire bandwidth of the electromagnetic spectrum is utilized ranging from X-ray diffraction techniques to nuclear magnetic resonance (NMR) methods. In a first hyphenation approach, AFM was combined with optical microscopy.<sup>6</sup> Optical microscopy (OM) can be largely grouped into far-field and near-field techniques; combinations taking advantage of near-field optical microscopies are discussed later in this Feature. Besides the need to localize the sample region of interest right underneath the AFM cantilever/probe, a dominating driving force toward hybrid AFM-OM systems is related to life science applications, where optical microscopy and its advanced techniques are already routine tools.<sup>7</sup> AFM is highly suitable for imaging biological samples such as live cells and tissues, as it can be operated in buffered solution and at controlled temperature conditions, thereby providing high-resolution imaging of structural surface features and analyzing forces in the pico- and nano-Newton regime even at individual cells, bacteria, virus particles, etc.

In the early days of AFM, the sample was typically mounted at the piezoelectric actuator (i.e., lead zirconium titanate (PZT) tube scanner) for translation in *x*-, *y*-, and *z*-direction, while the cantilever and the integrated deflection detection unit was fixed in an “AFM head” including a laser diode, mirrors, and a split photodetector analyzing the reflected laser beam. Most commercially available systems use a red-emitting laser diode (around 635–670 nm peak emission), as first described by IBM.<sup>8,9</sup> Hence, approaches combining AFM with inverted optical microscopy required that the objective can be moved in the *x*- and *y*-positions as well, while the objective was placed within the hollow PZT tube.<sup>10</sup> On the basis of this setup, an optical resolution of approximately 1 μm could be achieved with the sample located on a transparent substrate. Shortly thereafter, the first commercially available combined instrument was introduced in 1994 (Bioscope by Digital Instruments, now Bruker Corp.).

In the life sciences, fluorescence microscopy is considered a key optical technology, as molecule-specific fluorescent labeling including immunolabeling or fluorescent protein tags facilitates investigating the spatial distribution and dynamics of subcellular structures, proteins, or genomic sequences.<sup>11</sup> Hence, combining AFM with fluorescence microscopy is attractive, as high-resolution information on topographical features, forces, and/or elasticity ideally combines with high-resolution imaging of certain proteins in a complex matrix (e.g., a live cell), thereby enabling a more complete understanding of structure–function relationships in complex biological systems.

As the conventional laser diodes used in AFM systems are emitting around 635–670 nm, optical interferences during the detection of fluorescent species excited or emitting within this wavelength range are a potential problem. Filters have been introduced attenuating the laser radiation evident within the optical microscope images. Alternatively, low-coherence laser diodes emitting at infrared (IR) wavelengths (e.g., 850 nm) have been introduced for analyzing the deflection signal of the AFM cantilever.<sup>12</sup> Basically all commercial AFM systems offer the option of a combined AFM/optical platform with most combinations based on integrating the AFM functionality onto

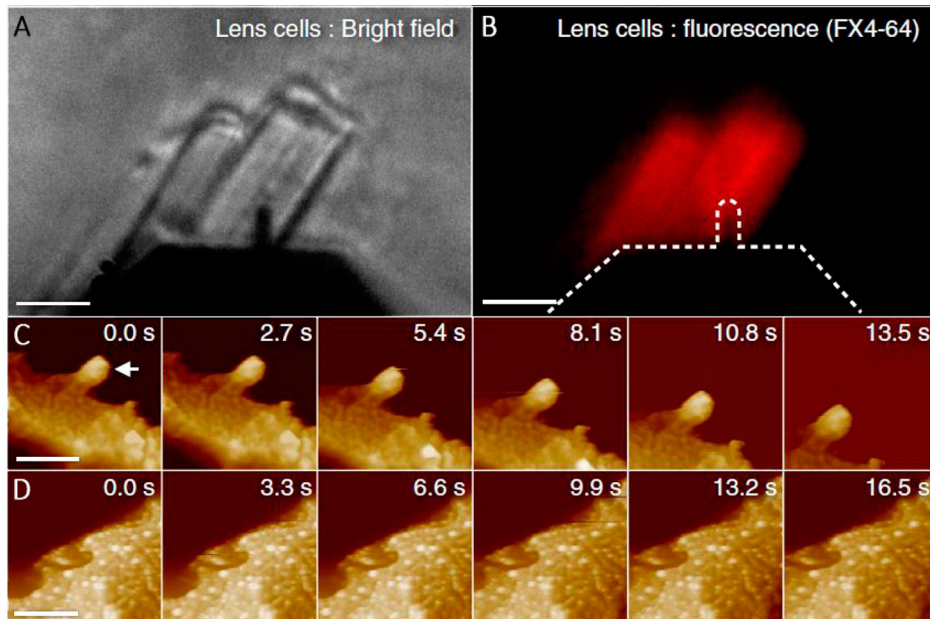


**Figure 2.** Combined high-speed AFM-OM imaging of native lens cells. (A) Bright field image and (B) fluorescence image (FX4-64 membrane staining) revealing the cantilever placed in the vicinity of lens cells (scale bars, 10  $\mu\text{m}$ ). Parts C and D show a series of high-speed AFM images of characteristic ball-and-socket structures at lens cells (arrow in part C) and surface hump and valley structures at the cell surfaces (scale bars, 2  $\mu\text{m}$ ). Reprinted with permission from ref 30. Copyright 2013 Macmillan Publishers Limited.

a state-of-the-art inverted microscope system accommodating the AFM scan head (with the cantilever mounted to the PZT scanner) using a customized sample stage. The utility of such hybrid systems for studying life cells, DNA, pathogens, microbes, and other biologically relevant species and entities has been documented.

Within the last decades, standard wide-field microscopy was increasingly augmented by more sophisticated optical techniques including Forster resonance energy transfer (FRET),<sup>13</sup> confocal laser scanning microscopy (CLSM),<sup>14</sup> total internal reflection fluorescence (TIRF),<sup>15</sup> and highest-resolution techniques such as photo activated localization microscopy (PALM)<sup>16</sup> or stochastic optical reconstruction microscopy (STORM)<sup>17</sup> facilitating subwavelength resolution beyond the diffraction limit, which is usually determined by the wavelength of the incident radiation and the numerical aperture of the optical components. For most of these advanced optical techniques, a combined approach with AFM has already been demonstrated, as recently summarized in a comprehensive review.<sup>18</sup>

Trache and Meininger have presented a hybrid instrument (NanoFluor),<sup>19</sup> which is suitable for studying cellular responses resulting from external chemical and/or mechanical stimulation (i.e., “mechanotransduction phenomena”). The quantitative assessment of cytoskeletal changes, binding probabilities, adhesion forces, and micromechanical properties is accessible via AFM, while the simultaneously obtained FRET, TIRF, or internal reflection microscopy (IRM) data provide insight on real-time dynamic changes during cell–substrate interactions. Super-resolution imaging techniques frequently termed optical nanoscopy such as stimulated emission depletion microscopy (STED),<sup>20</sup> PALM, or STORM are particularly suitable for imaging nanoscopic mammalian cell structures including microtubules, actin filaments, intermediate filaments (keratin), and neurofilaments.<sup>21</sup> Super-resolution imaging with hybrid techniques such as STED-AFM and STORM-AFM (schematic-

ally shown in Figure 1, left) have been demonstrated for, e.g., analyzing cytoskeletal structures of HeLa cells.<sup>22</sup>

A remaining challenge is the temporal synchronization of the simultaneously obtained optical and topographical data. In contrast to optical techniques, AFM is rather slow and provides comparatively low temporal resolution due to mechanical limitations in the cantilever scan rates using conventional probes. Hence, the correlation of dynamic cellular processes visualized via optical techniques with real-time observations related to surface modifications is difficult to achieve. To resolve this problem, recent promising developments pioneered by the groups of Hansma, Ando, and Miles<sup>23–25</sup> are focusing on hyphenating optical microscopy with high-speed AFM instrumentation enabling scanning the probe at video-rates, which facilitates the correlation with complementary optical data in the spatial as well as the temporal domain. The key development for increasing the scan speed was a reduction of mass and size of the cantilevers, which resulted in significantly increased resonance frequencies. In addition, the rigidity and stiffness of the motion translators (i.e., piezo-scanners) was improved, which enabled approaching the maximum scanning frequency in comparison to traditional PZT scanners, which are characterized by a limited bandwidth.<sup>26</sup> To that end, a variety of scanners suitable for high-speed AFM imaging have been introduced including the flexure scanner,<sup>27,28</sup> and novel methods for amplitude detection<sup>29</sup> in combination with improved optical deflection detection and accelerated data acquisition. A remaining caveat is that the cantilever scan speed and the dimension of the scanned surface area are inversely related, i.e., by increasing the scan speed a reduction in analyzed sample surface area has to be considered.

Scheuring and co-workers have recently demonstrated high-speed AFM combined with optical/fluorescence microscopy.<sup>30</sup> In contrast to most commercially available AFM-OM hybrid systems, in this approach the optical path is integrated into the AFM setup instead of mounting an AFM scan head onto an

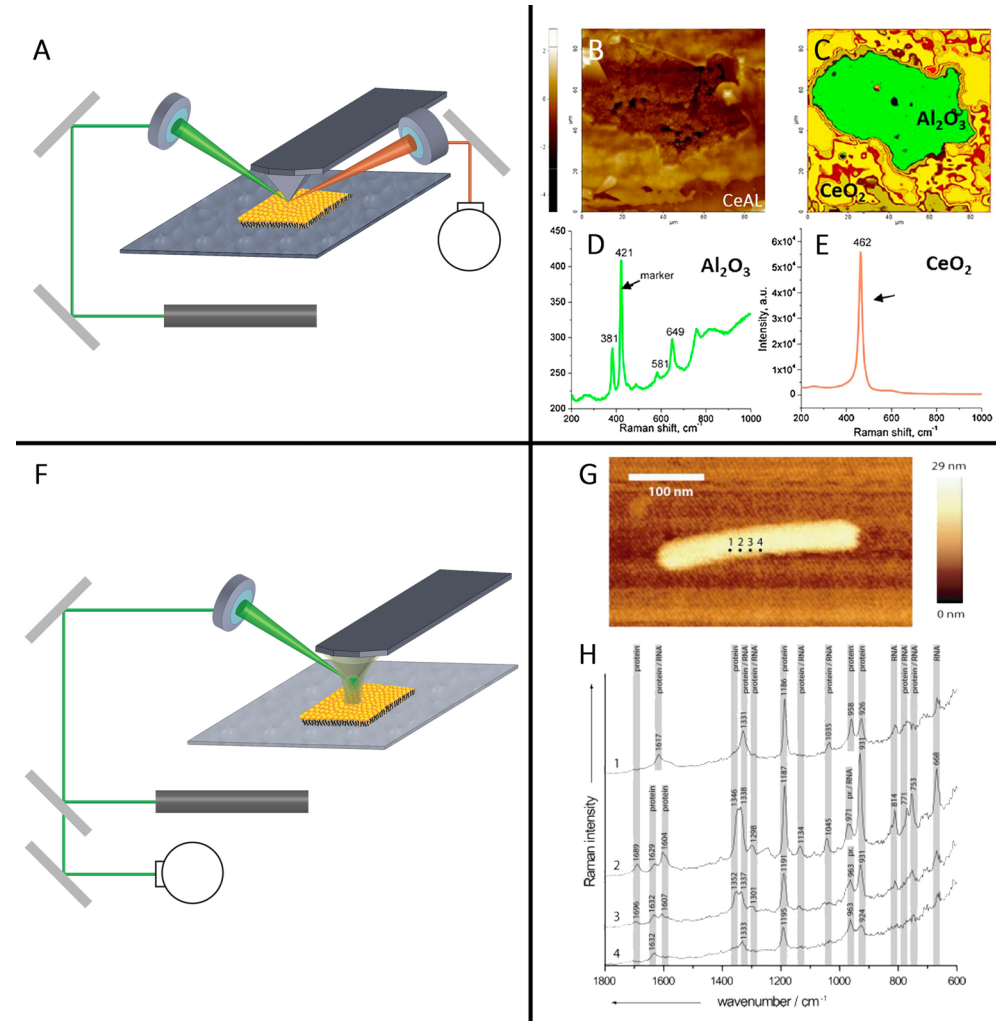


**Figure 3.** Far-field Raman-AFM setup with side illumination. (B–E) Heterogeneity of precalcined kanthal steel impregnated with ceria (CeAl sample) imaged by interfaced AFM-Raman microscopy; (B) AFM topography map; (C) Raman coupled map of the same area shown in part B obtained using (D,E) two marker bands of  $\alpha\text{-Al}_2\text{O}_3$  ( $421\text{ cm}^{-1}$ ) and  $\text{CeO}_2$  ( $462\text{ cm}^{-1}$ ). Reprinted with permission from ref 42. Copyright 2013 Elsevier. (F) TERS setup with side illumination. (G) AFM image of a tobacco mosaic virus imaged with a Ag-modified AFM tip. (H) Corresponding Raman spectra. The positions of the TERS tip in respect to the virus particle are marked. The TERS spectra of the virus particle are recorded at various positions. Reprinted with permission from ref 45. Copyright 2009 Wiley VCH.

inverted microscope. Consequently, only minimal compromises in the quality of the integrated optical microscopy functionality are complemented by unsurpassed high-speed AFM performance. The capabilities of this hybrid system were demonstrated by imaging individual eukaryotic membrane proteins and their dynamics at a speed of 960 ms per frame. As an example, the architecture of mammalian eye lens junctional microdomains is shown in Figure 2. The supramolecular organization of lens-specific aquaporin 0 (AQP0), which mediates the tight packing of fiber cells necessary for lens transparency could be imaged by high-speed AFM.

Finally, AFM in a top-down design was also combined with surface plasmon resonance (SPR)<sup>31</sup> and with ellipsometry.<sup>32</sup> Using these instrumental hyphenations, the kinetics of polymer film degradation were *in situ* studied.<sup>31</sup> As the gold-coated surface of the SPR element may also serve as an electrode, electropolymerization reactions were monitored for the example of conductive poly(3,4-ethylenedioxythiophene) (PEDOT) formation.<sup>33</sup>

## ■ AFM COMBINED WITH SPECTROSCOPY

While fluorescence-based optical techniques in the far- or near-field regime are powerful strategies for investigating dynamic processes in the life sciences, they also bear certain impediments. Usually, fluorescence microscopy requires labeling with specific fluorophores comprising appropriate excitation and emission characteristics for the visualization of selected targeted species and structures, e.g., within cells.<sup>34</sup> However, fluorescent labels may alter the biological sample, and for complex biological systems time-consuming and elaborate tests are necessary to exclude physiological effects of molecular or nanoparticulate marker structures. Furthermore, photobleaching other photophysical effects may in addition adversely affect the biological system. Finally, beyond applications in the life sciences, the utility of such studies, e.g., in high-resolution imaging of dynamic chemical processes is undoubtedly, but may not allow fluorescent labeling. Hence, a distinct need for label-free hybrid techniques is clearly evident.

Next to mass spectrometry and NMR, vibrational spectroscopies are routinely used in chemistry to obtain molecule-

specific information. Raman and infrared spectroscopy are considered among the most important nondestructive and label-free routine optical analysis tools providing molecular information even in complex matrixes. The fingerprint region considered in the range of 1200–600 cm<sup>-1</sup> is highly suitable for the identification of organic constituents. In analogy to the optical techniques discussed so far, conventional vibrational spectroscopy in the far-field remains diffraction-limited. However, within recent decades tremendous progress has been achieved on facilitating spatially resolved vibrational spectroscopic information taking advantage of scanning probes.<sup>35,36</sup> Initially, this approach has been demonstrated for optical microscopy techniques such as aperture-less near-field scanning optical microscopy (NSOM), which is based on conventional AFM technology<sup>37</sup> illuminating the apex of a suitable AFM tip with electromagnetic radiation. The advantage of combining spectroscopic data with topological information is immediately evident and nowadays applied across many disciplines ranging from surface sciences to biomedical research.

The Raman principle, which was first described by Sir C. V. Raman in 1928, is based on inelastic scattering of radiation in the visible to near-infrared region of the electromagnetic spectrum. However, the scattering cross-section is up 14 orders of magnitude smaller than the signal intensity of elastic Raleigh scattering or fluorescence. High-powered laser or sufficiently long excitation times have to be used to generate suitable analytical signals. Nonetheless, Raman spectroscopy and confocal Raman microscopy are routine characterization tools in material sciences and in bioanalytical chemistry. For example, Raman spectroscopy is particularly useful for the characterization of carbonaceous materials such as carbon nanotubes and graphene.<sup>38,39</sup> The combination of Raman techniques with AFM is straightforward; therefore, different instrumental realizations including on-axis laser illumination, side illumination (exemplarily shown in Figure 3A), and in-line illumination using an inverted configuration have been implemented.<sup>40,41</sup> In this combination, the spatial resolution of the spectroscopic data is determined by the optical diffraction limit like in conventional confocal microscopy, which is dependent on the laser wavelength, the applied objective, and the confocal coupling. For a laser emitting in the visible range, the achievable spatial resolution is approximately 200 nm. Although the spatial resolution is not comparable with the resolution achieved in AFM, this combination transitioned into a routine tool in instrumental analysis. As an example, AFM and simultaneously obtained Raman maps of heterogeneous catalytic materials are shown in Figure 3B–E.<sup>42</sup> The AFM image of precalcined kanthal steel, which was impregnated with ceria shows that the sample surface was not evenly covered with ceria washcoat evident as regions with different texture (Figure 3B). The Raman maps prove the presence of CeO<sub>2</sub> (yellow and red) in the laminated area and  $\alpha$ -Al<sub>2</sub>O<sub>3</sub> (green) in the central region (Figure 3C). Figure 3D,E provides exemplary spectra for  $\alpha$ -Al<sub>2</sub>O<sub>3</sub> and CeO<sub>2</sub>, respectively.

Within the last 2 decades, significant progress in signal intensity has been achieved based on utilizing surface enhancement effects generated at rough conductive surfaces, a.k.a. surface enhanced Raman spectroscopy (SERS),<sup>43</sup> which was first demonstrated for adsorbed pyridine at electrochemically roughened Ag resulting in a signal enhancement by a factor of 10<sup>6</sup>.<sup>44</sup>

Generally, molecules adsorbed at nanometer-sized metal particles experience a locally enhanced electromagnetic (EM) field, thereby resulting in a significant enhancement of their vibrational signatures up to several orders of magnitude.<sup>46</sup> It has been demonstrated that elongated particles, mostly Ag or Au, with a particle size of 10–100 nm reveal the most pronounced enhancement effects. Enhancement effects were also observed if a metallic probe (such as an etched wire) or metal-coated AFM tips were brought into close contact with a sample surface providing adsorbed molecules of interest.<sup>47,48</sup> If the metallic probe is placed within a distance <10 nm to the sample surface, Raman spectra may be obtained beyond the diffraction limit, and therefore, chemical and structural information on the surface composition and topography both at high resolution can be achieved.

Surface enhancement using a sharp metallic tip is termed tip-enhanced Raman spectroscopy (TERS), which combines the enhanced sensitivity and chemical information on SERS with the spatial resolution achievable in scanning probe microscopy.<sup>49</sup> Surface plasmons excited at the apex of the AFM tip by a focused laser beam lead to strong interactions with the molecules in the vicinity of the metal tip, thus resulting in a highly localized and significantly enhanced Raman signal. In analogy to SERS, a chemical effect is observed, which is related to an amplified polarizability of the molecule due to a charge transfer between the metal and the adsorbed molecule.<sup>50</sup> The intensity of Raman scattering is directly proportional to the square of the induced dipole moment,  $\mu_{\text{ind}}$ . The induced dipole moment is determined by the polarizability ( $\alpha$ ) and the magnitude of the incident electromagnetic field ( $E$ ). However, the chemical effect is much less pronounced compared to the electromagnetic effect.

In respect to instrumental hyphenations, several approaches have been developed. In general, laser light is focused onto the apex of the tip, and scattered light is frequently collected via the same high-numerical aperture objective. A notch filter is commonly used to reduce the Rayleigh-scattered light. The Stokes and anti-Stokes signal is then focused and directed to the detector of a spectrometer. TERS is usually operated in reflection or in confocal mode depending on the transparency of the investigated sample. For opaque samples, the reflection mode with top or side illumination (Figure 3F) using a long working distance objective is routinely applied, whereas for transparent samples, similar to optical microscopy, an inverted microscope with in-line illumination is used. For combined AFM, imaging may be performed in contact, dynamic, and noncontact mode using, e.g., a tuning-fork read-out mechanism. Chemical and topological resolution down to 12 nm has been reported.<sup>51</sup> In terms of applications, TERS has gained significant popularity and has been employed predominantly in material sciences and bioanalytical research including investigations in UHV to imaging in solution. Although in vitro imaging of biological samples is experimentally more challenging, the number of bioanalytical applications is continuously increasing due to the breadth of information, which can be obtained.<sup>52</sup> Figure 3G shows the AFM image and Figure 3H the corresponding Raman data of a single tobacco mosaic virus.<sup>45</sup>

The obtained Raman spectra may be highly convoluted especially in complex biological matrixes and therefore difficult to interpret. Besides the combination with AFM, hybrid approaches have been demonstrated using wire probes, STM tips, and near-field optical probes.<sup>41</sup> For example, Zhang and

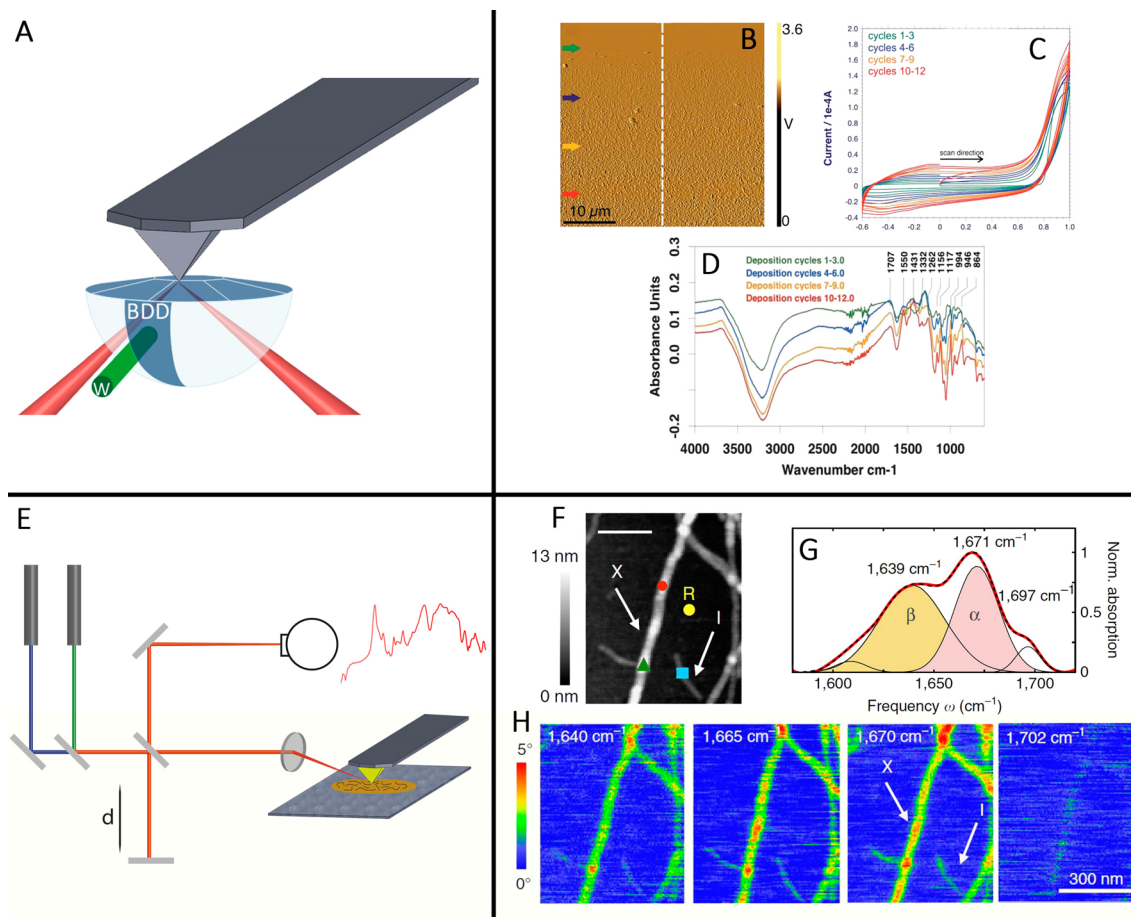


**Figure 4.** (A) Scheme of combined IR-ATR-AFM setup for spectroelectrochemistry in the mid-infrared region. (B) Deflection image recorded in contact mode during polymerization cycles of EDOT. (C) Cyclic voltammograms recorded for the deposition of PEDOT (four deposition sets indicated by different colors with three cycles for each set applied). (D) Obtained IR-ATR spectra after 3, 6, 9, and 12 deposition cycles: increasing number of cycles from top to bottom. Reprinted with permission from ref 57. Copyright 2013 Royal Society of Chemistry. (E) Schematic representation of the near-field IR-approach based on the scattering approach. (F) Topography of insulin fibrils on a silicon substrate. Scale bar: 200 nm. The arrows indicate a type I fibril (I) and a 9 nm-thick fibril composed of several protofilaments (X). (G) Band decomposition of the nano-IR spectrum (red curve) based on five absorption bands (thin black curves). The dashed black curve shows the resulting fit. (H) s-NSOM phase images of the fibrils shown in part F recorded at different wavenumbers; scale bar: 300 nm. Reprinted with permission from ref 58. Copyright 2013 Macmillan Publishers Limited.

co-workers demonstrated single molecule resolution of submonolayered meso-tetrakis(3,5-ditertiarybutylphenyl)-porphyrin ( $H_2$ TBPP) molecules at an Ag(111) surface in UHV and at low temperature.<sup>53</sup>

Although this hybrid technique appears highly useful, the experimental realization is frequently challenging due to the still limited reliability of TERS tip fabrication. As the achievable enhancement effect is strongly dependent on the dimensions and geometry of the nanosized structure at the apex of the metallized AFM tip, any change due to contact during the measurements may have an adverse effect on the Raman response. Not only adsorption of molecules at the tip may alter the Raman signal, also chemical modification or geometrical alteration has an impact, which is critical for reliable and reproducible measurements, and in particular for signal quantification. Silver is known to show the highest enhancement factor, however, in comparison to gold it remains more prone to oxidation. In addition, local heating due to strong electromagnetic fields at the tip apex may lead to additional changes of the tip properties. A review focusing in detail on these challenges and tip requirements was recently published among others by the Zenobi group.<sup>35</sup>

Alternatively, IR spectroscopy, which is also a label-free technique, provides a wealth of qualitative and quantitative chemical and structural information with high molecular selectivity. In the mid-infrared region (MIR) of the electromagnetic spectrum (3–25 μm), fundamental vibrational modes of molecules are directly excited via appropriate photon absorption. Similar to Raman signatures, the analysis of organic constituents benefits from the so-called “fingerprint” region (10–15 μm) providing distinct absorption patterns characteristic for almost any organic species. In contrast to Raman spectroscopy, water absorptions represent a problem for in situ IR spectroscopy due to strong absorption bands around 1640 and 3400 cm<sup>-1</sup>. Infrared attenuated total reflection spectroscopy (IR-ATR) minimizes this problem, as the obtained analytical signal is limited to the penetration depth of the evanescent field.<sup>54</sup> If IR radiation is coupled into an internal reflection element at angles exceeding the critical angle, the radiation propagates within this optical waveguide due to total internal reflection. Depending on the refractive index contrast between the optical waveguide and the adjacent medium, the evanescent field penetrates to a certain extent into the surrounding medium. The evanescent field is characterized by

an exponentially decaying intensity with increasing distance to the waveguide/sample interface. Hence, typical penetration depths of few micrometers ( $\mu\text{m}$ ) are obtained in the MIR.<sup>46</sup> IR-absorbing molecules present in close vicinity to the waveguide surface may interact with photons similar to transmission absorption spectroscopy, thereby resulting in evanescent field absorption spectra.

Similar to hybrid Raman-AFM systems, also combined IR-AFM approaches have been reported either utilizing far-field or near-field strategies. In terms of spatial resolution, the far-field approaches are again diffraction-limited, and the achievable spatial resolution is governed by the wavelength of the electromagnetic radiation, which evidently results in several micrometers of spatial resolution in the MIR. Combining AFM with IR-ATR is straightforward, as a top-down AFM may again be easily combined with an IR-ATR setup using the waveguide as the sample substrate for AFM investigations, while molecules may be simultaneously probed by the evanescent field, as shown in Figure 4B and D. A simultaneous acquisition of topographical information by AFM and infrared evanescent field absorption spectra via IR-ATR is achieved.<sup>55,56</sup> A significant advantage of this configuration is the fact that IR-ATR spectroscopy is not influenced by the presence of the AFM tip. Furthermore, studies may be readily performed in solution, which is critical for biorelated research. For example, high-resolution topographical information on phase transitions in materials or conformational changes of molecules adsorbed at the ATR crystal surface can be studied by AFM, while molecular changes due to chemical reactions or dynamic processes can be simultaneously detected with IR.<sup>55</sup> However, the IR information is collected across the entire area of the ATR crystal, and locally confined changes may not be detected in this configuration. Only a limited selection of MIR transparent materials such as ZnSe, ZnS, Ge, diamond, or Si are available for such combined approaches. Recently, a mid-infrared transparent electrode based on a thin boron-doped diamond layer deposited onto a diamond ATR crystal has been demonstrated in a hybrid IR-ATR-AFM system (Figure 4A).<sup>57</sup> Combined AFM-spectroelectrochemical studies were demonstrated for the *in situ* characterization of a polymerization reaction (i.e., (PEDOT), as shown in Figure 4B (AFM deflection image), part C (corresponding cyclic voltammogram for the electropolymerization of EDOT), and part D (IR spectra revealing the changes due to the polymerization progress).

Yip and co-workers investigated protein–membrane interactions with a combined IR-ATR-AFM setup using a multireflection germanium ATR crystal.<sup>56</sup> The gel–fluid phase transition due to heating and cooling of multilamellar lipid bilayers was simultaneously mapped with AFM (i.e., change in topography due to heating and cooling cycles of the sample), while the vibrational information could elucidate changes in inter- and intramolecular bonding. A recent review of the same group focuses on the advantages of far-field and near-field MIR spectroscopy in membrane physics.<sup>59</sup>

In contrast to near-field Raman, in IR spectroscopy two distinctly different near-field (now termed “nano-IR”) approaches have been developed. Keilmann and co-workers pioneered an approach using a hybrid system taking advantage of a metalized AFM probe, which serves as a scattering element for MIR laser radiation (schematic representation in Figure 4E). This technique was termed scattered near-field optical microscopy (s-NSOM).<sup>60</sup> This approach was further evolved

implementing a Michelson interferometer. Early applications of scanning near-field infrared microscopy (SNIM) have focused on chemical mapping of thin films and polymers. Recently, Hillenbrand and co-workers demonstrated a spatial resolution of 20 nm for mapping poly(methyl methacrylate) (PMMA) on a silicon sample.<sup>61</sup> The system is equipped with laser-based infrared continuum light source providing sufficient power for detecting the weak molecular vibrational resonances of organic samples.

An alternative approach based on a different physical principle was introduced by Dazzi et al.<sup>62</sup> Here, the AFM tip was used as a detector for localized thermal changes induced by the absorption of radiation via molecules present at an optical waveguide surface. Similar to ATR techniques, an IR beam illuminates the sample by total internal reflection. Molecular vibrations within the evanescent field lead to a highly localized thermal expansion, which in turn excites the AFM cantilever to oscillate resonantly. From the ringdown pattern of the cantilever oscillation, localized IR absorption spectra can be extracted, while the oscillation frequencies are related to the stiffness of the sample. Both approaches have in common that the resolution is no longer determined by the wavelength of the radiation but by the radius of curvature of the AFM tip, which is typically in the range of 10–20 nm.<sup>63</sup>

Nano-IR and TERS are certainly among the most advanced combined AFM techniques, which have already been commercialized and which are applied in a variety of cutting-edge research areas ranging from catalysis to biomedical applications including protein identification. An example for the bioanalytical relevance is shown in Figure 4F–H. The protein conformation within individual insulin fibrils was studied with nano-IR.<sup>58</sup> Insulin may form amyloid-like fibrils and fibers composed of filament-shaped protein aggregates. Nano-IR enables to detect and image the secondary structure with approximately 30 nm lateral resolution, as shown in Figure 4H. Although superior resolution at complex samples may be obtained, only few studies at a defined solid–liquid interface have been demonstrated for TERS to date.<sup>64,65</sup> For nano-IR, an additional challenge remains, the availability of appropriate tunable IR laser light sources, which may be resolved with the availability of increasingly tunable quantum cascade lasers (QCLs). So far, most applications utilizing AFM tip-based scattering approaches have been demonstrated either in air or vacuum. Likewise, near-field IR studies have not been shown in solution in the literature.

## ■ COMBINATIONS WITH SCANNING PROBE TECHNIQUES

The hyphenation of AFM with complementary scanning probe techniques is attractive for probing solid/liquid interfaces. There are emerging problems in the corrosion sciences with surface processes, e.g., leading to topological and activity changes but also in heterogeneous catalysis and biomedical research, where, e.g., altered concentrations of signaling molecules may be related to pathological behavior. Consequently, the development of hyphenated scanning probe techniques, which next to physical parameters provide information on local concentration changes of certain molecules, are of ubiquitous interest. Complementary information in hyphenated SPM techniques is typically obtained by integrating additional functionality tight within the AFM probe.<sup>66</sup> Among others, some of the established AFM modes including magnetic force microscopy, scanning thermal

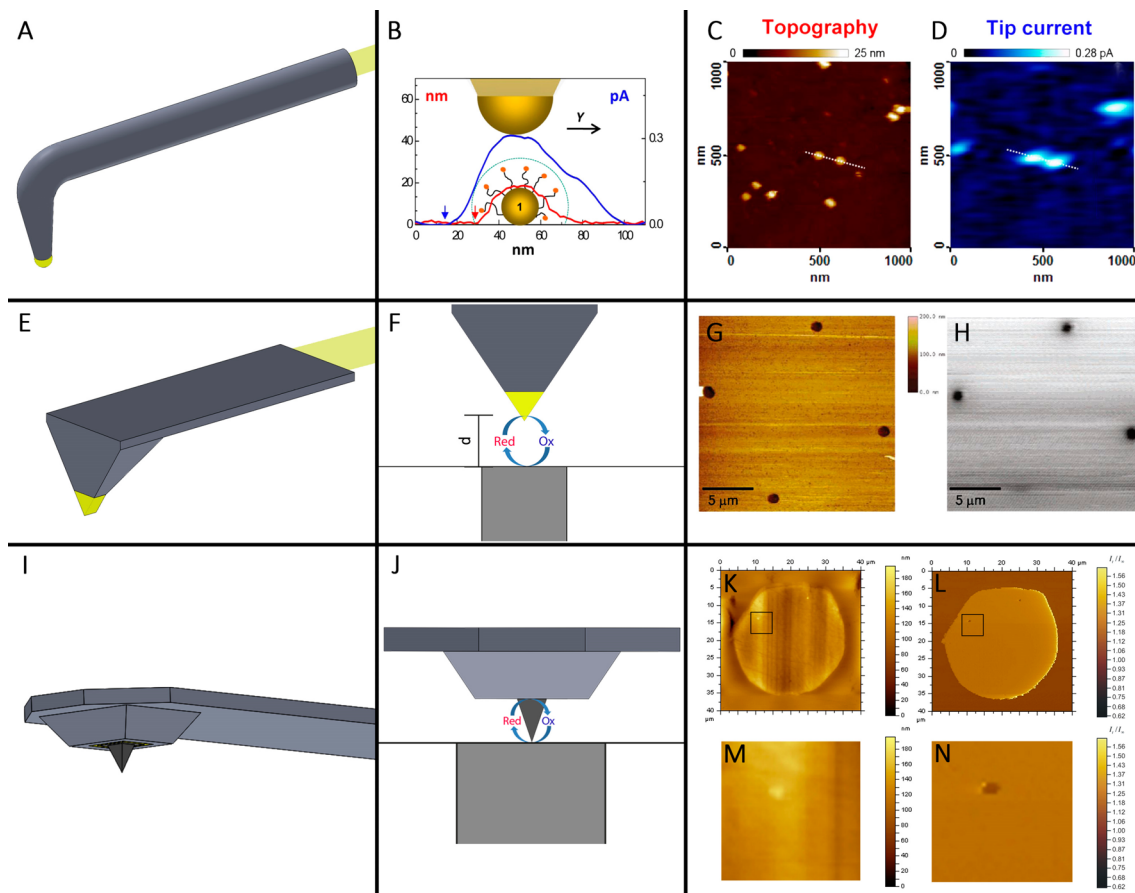


**Figure 5.** (A) Scheme of cantilever-shaped conical microelectrode. (B) Schematic representation of simultaneously mapping the topography and electrochemical response of redox-labeled nanoparticles. (C) AFM-SECM images of  $\sim 20$  nm sized gold nanoparticles functionalized with redox-labeled PEG chains. Images were recorded in dynamic mode AFM. Reprinted from ref 73. Copyright 2013 American Chemical Society. (E) Scheme of a microfabricated conical AFM-SECM probe. (F) Schematic representation of feedback imaging with a combined conical AFM-SECM probe. (G,H) AFM-SECM images recorded sequentially. For topographical imaging, the tip was held in contact with the surface (unbiased), while electrochemical data were acquired with the tip imaging at a fixed height of 1  $\mu\text{m}$  from the surface of the substrate. Reprinted from ref 76. Copyright 2005 American Chemical Society. (I) Combined AFM-SECM probe with recessed electrode. (J) Schematic view of combined imaging. (K,L) Topography and simultaneously recorded electrochemistry with a reshaped AFM tip height of 800 nm. (M,N) Magnified view of an insulating diamond particle in topography and electrochemical image, respectively. Reprinted with permission from ref 77. Copyright 2012 Elsevier.

microscopy, electrostatic force microscopy, and Kelvin force microscopy are based on functionalized or sophisticated scanning probes or probe designs.<sup>67</sup>

Adding electrochemical functionality is of interest for monitoring and imaging dynamic *in situ* processes and for obtaining heterogenic rate constants. Scanning electrochemical microscopy (SECM), a derivative of STM, was introduced by Bard in 1986 and uses microelectrodes for obtaining laterally resolved electrochemical information.<sup>68,69</sup> In SECM, the localized information is based on voltammetric or potentiometric measurements at microscopic or nanoscopic electrodes, which are positioned in close proximity (i.e., several electrode radii) to the sample surface. Among other factors such as distance and active electrode radius, the electrochemical signal is strongly dependent on the nature of the sample surface and on occurring surfaces processes. In contrast to other members of the SPM family, a thorough theoretical treatment was developed for SECM enabling an exhaustive theoretical description of the involved processes. Only within the past decade, a significant body of literature appeared using nanosized electrodes for imaging in SECM, as recently reviewed.<sup>66</sup> This delay in improving the spatial resolution in imaging electrochemistry is related to the fact that in

conventional SECM the tip (i.e., the electrode) is usually scanned in a constant height across the sample surface. As the distance between tip and sample is related to the size of the electrode (which refers that the distance decreases with the decreasing radius of the active electrode), microelectrodes were used for most imaging experiments. The obtained electrochemical signal is not only dependent on the electroactivity of the sample surface but also on the actual distance, which may lead to convoluted electrochemical and topographical data if submicrometer-sized electrodes are used.

Adding electrochemical functionality to AFM probes was initiated by Unwin and MacPherson<sup>70</sup> presenting a cantilever-shaped conical electrode (Figure 5A), which was later also adopted by others<sup>71</sup> and used as a combined probe for AFM-SECM measurements such as imaging pore transport<sup>72</sup> or, as shown in Figure 5C,D, for imaging redox-labeled nanoparticles.<sup>73</sup> Shortly thereafter, an AFM-SECM combination based on microfabrication processes was realized by Kranz and collaborators enabling the reproducible microfabrication of AFM-SECM probes (Figure S1).<sup>74</sup> On the basis of these fundamental studies, several approaches have later been introduced, which can be categorized as combined AFM-SECM probes with the electroactive area at the apex of an AFM

tip, and microfabricated probes with a recessed frame-, disc- or ring-shaped electrode integrated at a defined distance from a nonconductive AFM tip. An advantage of the recessed-type probes is certainly that topographical and electrochemical response may be obtained in a truly simultaneous fashion and that the integrated electrode may be further modified with functional layers. Combined probes with the electroactive area at the apex of the tip can be subdivided into cantilever-shaped conical electrodes, which are typically fabricated by wet-etching followed by an electrochemical insulation process and micro-fabricated probes (Figure 5E) typically processed in a cleanroom environment.<sup>75,76</sup> For AFM-SECM probes with the electroactive area at the tip apex, sequential imaging as shown in Figure 5G,H for patterned microelectrodes might be necessary. Common to all these approaches is that the combined probes require a well-defined tip apex with a small radius of curvature (in the range of 20–30 nm) enabling high-resolution AFM imaging, a force constant comparable to commercially available AFM probes, a well-defined integrated electroactive area, and a pinhole-free insulation of the entire probe avoiding any leakage currents, which would lead to erroneous electrochemical information.

An intriguing aspect of hyphenated AFM-SECM is certainly that most well-established electroanalytical techniques ranging from polarographic and potentiometric methods to advanced techniques such as fast-scan voltammetry may be performed at such combined AFM-SECM probes and that a wide variety of electrode materials including, e.g., boron-doped diamond (BDD) may be readily integrated.<sup>77</sup> Simultaneously recorded AFM-SECM images of a disc-microelectrode structure obtained via an AFM tip-integrated BDD electrode are shown in Figure 5K,L (zoomed view parts M,N). In addition, appropriate surface modification of such integrated electrodes facilitates enhanced imaging modalities ranging from tip-integrated biosensors<sup>78</sup> for mapping biologically relevant molecules to attaching redox-labels, as demonstrated by Demaille and co-workers.<sup>79</sup> Finally, a triple SPM combination, AFM-NSOM-SECM, was presented by Ueda et al. and was applied for imaging neurites of living PC12 cells.<sup>80</sup>

A limiting factor, which has probably prevented a more widespread adoption of AFM-SECM to date is certainly related to the fact that neither a commercial AFM-SECM instrument nor combined AFM-SECM probes are commercially available. However, it is anticipated that suitable instrumentation will be introduced in the not too distant future.

## ■ COMBINATION WITH MASS-SENSITIVE TECHNIQUES

The quartz microbalance is an *in situ* analytical technique offering nanogram sensitivity, which translates into the detection of submonolayer surface coverage.<sup>81</sup> This label-free quantitative method is frequently applied for investigating dynamic electrode processes, studying corrosion phenomena, and for biosensing applications due to its superior sensitivity. Typically, gold-coated AT-cut quartz crystals are used in QCM. The oscillation frequency of the crystal decreases if the crystal is loaded with rigid mass following the Sauerbrey relation.<sup>82</sup> In addition, the viscoelastic properties of deposited films can be studied, as the resonant frequency depends on the viscoelastic properties of the crystal and of the adjacent phase, as determined by the coupling boundary conditions. Damping of the oscillation is typically associated with changes in the material elasticity, which is dependent on particle size and

shape. The evaluation of QCM data beyond the simple application as a mass-sensing device in air is quite complex and requires sophisticated models related to the impedance behavior of the entire system (i.e., electric branch and acoustic branch). The combination with AFM may complement the data interpretation in QCM. For example, combined QCM-AFM studies were shown for cell adhesion on polyurethane films<sup>83</sup> and for the investigation of the adsorption of ferritin.<sup>84</sup> As the resonator consists of a gold layer, the combination of QCM-AFM for investigating *in situ* electrochemical processes is immediately evident.<sup>85</sup>

Mass spectrometry is the unrivaled analytical tool for identifying and characterizing organic, biological, and bio-inorganic molecules in complex (e.g., biological) matrixes down to attomolar concentration levels. The most recent advances in mass spectrometry facilitate probing samples even at ambient conditions.<sup>86</sup> So far, no hybrid AFM-MS has been realized; however, two groups have independently presented approaches utilizing scanning microprobes (i.e., capillaries) for localized electrospray experiments.<sup>87,88</sup> MS analysis of biological samples was enabled by introducing small movable microfabricated capillaries with inner diameters of 10–50 μm of the collection channel and an 8–20 μm diameter of the microspray orifice.<sup>87</sup> An alternative approach using commercially available capillaries was recently demonstrated.<sup>88</sup> Here, the capillary probe was positioned using optical techniques (high speed video imaging or laser metering) and was used to desorb sample constituents at atmospheric conditions, which were then collected by the nozzle of a mass spectrometer.<sup>85</sup>

An interesting concept (Figure 6) was very recently demonstrated by Ovchinnikova et al.<sup>89</sup> This hybrid atomic

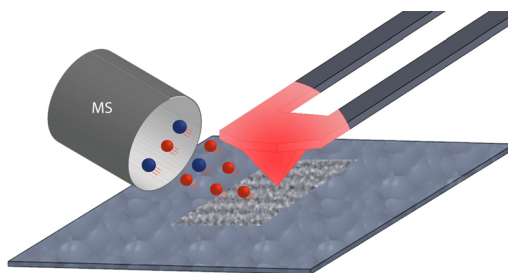


**Figure 6.** Schematic of the localized desorption using a heatable AFM probe. Adapted from ref 89. Copyright 2014 American Chemical Society.

force microscopy-atmospheric pressure mass spectrometry imaging system is based on heatable probes enabling a localized thermal desorption of sample constituents. Coupling local desorption to atmospheric pressure chemical ionization and mass analysis, the detection of a specific bacterial metabolite (phenazine-1-carboxamide) desorbed from a live bacterial colony of *Pseudomonas* species GM17 immobilized on an agar gel was demonstrated.

In conclusion, if analytical chemists could design an ideal analytical instrument, they would probably wish for a device providing chemical identification at trace-level concentrations suitable for studying rapid transient processes ideally with high lateral resolution in real-world samples without any sample pretreatment. The multitude of papers published every year focusing on developments targeting sophisticated combined instrumentation clearly corroborates the need of and efforts toward such advanced hybrid instrumentation. Even though it

remains open whether any tool will ever fulfill the entire wish list of advanced analytical chemists, it may safely be anticipated that within the next decade exciting hyphenated analytical techniques will be emerging based on combined scanning probe microscopies.

## AUTHOR INFORMATION

### Corresponding Author

\*E-mail: christine.kranz@uni-ulm.de. Phone: (+49) 7315022479. Fax: (+49) 7315022463.

### Notes

The authors declare no competing financial interest.

### Biographies

A. Eifert is currently a graduate student at IABC working on combined AFM-SECM with the focus on integrated boron-doped diamond electrodes and their application for the localized detection of biomolecules.

C. Kranz is a tenured researcher at the Institute of Analytical and Bioanalytical Chemistry (IABC), University of Ulm. Her current research focuses on scanning probe microscopy, scanning electrochemical microscopy (SECM), multifunctional scanning probes (e.g., combination AFM-SECM), and combined (nano)analytical systems integrating scanning probe microscopy with mid-infrared spectroscopy. In addition, she is heading the Focused Ion Beam Center UUlm with a main interest in FIB-based microfabrication. Besides this instrumental focus, her research also involves in the development of miniaturized biosensors for medical applications such as localized ATP measurements at live cells.

## ACKNOWLEDGMENTS

The authors would like to acknowledge the Baden-Württemberg Stiftung within the project "Methoden für die Lebenswissenschaften" and the Boehringer Ingelheim-Ulm University Biocenter (BIU) for funding of related research at IABC.

## REFERENCES

- (1) Hirschfeld, T. *Anal. Chem.* **1980**, *52*, 297A–312A.
- (2) Binnig, G.; Quate, C. F.; Gerber, C. *Phys. Rev. Lett.* **1986**, *56*, 930–933.
- (3) Giessibl, F. J. *Jpn. J. Appl. Phys.* **1994**, *33*, 3726–3734.
- (4) Hosseini, B. H.; Louban, I.; Djandji, D.; Wabnitz, G. H.; Deeg, J.; Bulbul, N.; Samstag, Y.; Gunzer, M.; Spatz, J. P.; Hä默ling, G. J. *Proc. Natl. Acad. Sci. U.S.A.* **2009**, *106*, 17852–17857.
- (5) Albrecht, T. R.; Akamine, S.; Carver, I. E.; Quate, C. F. *J. Vac. Sci. Technol. A* **1990**, *8*, 3386–3396.
- (6) Hansma, P. K.; Drake, B.; Grigg, D.; Prater, C. B.; Yashar, F.; Gurley, G.; Elings, V.; Feinstein, S.; Lal, R. *J. Appl. Phys.* **1994**, *76*, 796–799.
- (7) Stephens, D. J.; Allan, V. J. *Science* **2003**, *300*, 82–86.
- (8) Meyer, G.; Amer, N. M. *Appl. Phys. Lett.* **1988**, *53*, 1045–1047.
- (9) Alexander, S.; Hellmans, L.; Marti, O.; Schneir, J.; Elings, V.; Hansma, P. K. *J. Appl. Phys.* **1989**, *65*, 164–167.
- (10) Putman, C. A. J.; van der Werf, K. O.; de Groot, B. G.; van Hulst, N. F.; Segerink, F. B.; Greve, J. *Rev. Sci. Instrum.* **1992**, *63*, 1914–1917.
- (11) Lippincott-Schwartz, J.; Patterson, G. H. *Science* **2003**, *300*, 87–91.
- (12) Geisse, N. A. *Mater. Today* **2009**, *12*, 40–45.
- (13) Forster, T. *Ann. Phys.* **1947**, *2*, 55–75.
- (14) Cremer, T. *Microsc. Acta* **1978**, *81*, 1–14.
- (15) Axelrod, D. *J. Cell Biol.* **1981**, *89*, 141–145.
- (16) Betzig, E.; Patterson, G. H.; Sougrat, R.; Lindwasser, O. W.; Olenych, S.; Bonifacino, J. S.; Davidson, M. W.; Lippincott-Schwartz, J.; Hess, H. F. *Science* **2006**, *313*, 1642–1645.
- (17) Rust, M. J.; Bates, M.; Zhuang, X. *Nat. Methods* **2006**, *3*, 793–796.
- (18) Moreno Flores, S.; Toca-Herrera, J. L. *Nanoscale* **2009**, *1*, 40–49.
- (19) Trache, A.; Meininger, G. A. *J. Biomed. Opt.* **2014**, *10*, 064023/1–064023/17.
- (20) Hell, S. W.; Wichmann, J. *Opt. Lett.* **1994**, *19*, 780–782.
- (21) Heilemann, M.; van de Linde, S.; Schüttel, M.; Kasper, R.; Seefeldt, B.; Mukherjee, A.; Tinnefeld, P.; Sauer, M. *Angew. Chem., Int. Ed.* **2008**, *47*, 6172–6176.
- (22) Chacko, J. V.; Zanacchi, F. C.; Diaspro, A. *Cytoskeleton* **2013**, *70*, 729–740.
- (23) Ando, T.; Kodera, N.; Takai, E.; Maruyama, D.; Saito, K.; Toda, A. *Proc. Natl. Acad. Sci. U.S.A.* **2001**, *98*, 12468–12472.
- (24) Walters, D. A.; Cleveland, J. P.; Thomson, N. H.; Hansma, P. K.; Wendman, M. A.; Gurley, G.; Elings, V. *Rev. Sci. Instrum.* **1996**, *67*, 3583–3590.
- (25) Humphris, A. D. L.; Miles, M. J.; Hobbs, J. K. *Appl. Phys. Lett.* **2005**, *86*, 034106/1–034106/3.
- (26) Schitter, G.; Astrom, K. J.; DeMartini, B. E.; Thurner, P. J.; Turner, K. L.; Hansma, P. K. *IEEE Trans. Control Syst. Technol.* **2007**, *15*, 906–915.
- (27) Fantner, G. E.; Schitter, G.; Kindt, J. H.; Ivanov, T.; Ivanova, K.; Patel, R.; Holten-Andersen, N.; Adams, J.; Thurner, P. J.; Rangelow, I. W.; Hansma, P. K. *Ultramicroscopy* **2006**, *106*, 881–887.
- (28) Picco, L. M.; Dunton, P. G.; Ulcinas, A.; Engledew, D. J.; Hoshi, O.; Ushiki, T.; Miles, M. J. *Nanotechnology* **2008**, *19*, 384018/1–384018/6.
- (29) Ando, T.; Uchihashi, T.; Fukuma, T. *Prog. Surf. Sci.* **2008**, *83*, 337–437.
- (30) Colom, A.; Casuso, I.; Rico, F.; Scheuring, S. *Nat. Commun.* **2013**, *4*, 21553–21561.
- (31) Shakesheff, K. M.; Chen, X.; Davies, M. C.; Domb, A.; Roberts, C. J.; Tendler, S. J. B.; Williams, P. M. *Langmuir* **1995**, *11*, 3921–3927.
- (32) Karageorgiev, P.; Orendi, H.; Stiller, B.; Brehmer, L. *Appl. Phys. Lett.* **2001**, *79*, 1730–1732.
- (33) Baba, A.; Knoll, W.; Advincula, R. *Rev. Sci. Instrum.* **2006**, *77*, 064101/1–064101/6.
- (34) Lichtman, J. W.; Conchello, J.-A. *Nat. Meth.* **2005**, *2*, 910–919.
- (35) Stadler, J.; Schmid, T.; Zenobi, R. *Nanoscale* **2012**, *4*, 1856–1870.
- (36) Bründermann, E.; Havenith, M. *Annu. Rep. Sect. C* **2008**, *104*, 235–255.
- (37) Mannoni, A.; Quercioli, F.; Tiribilli, B.; Ascoli, C.; Baschieri, P.; Frediani, C. *J. Lightwave Technol.* **1998**, *16*, 388–394.
- (38) Vannier, C.; Yeo, B.; Melanson, J.; Zenobi, R. *Rev. Sci. Instrum.* **2006**, *77*, 023104/1–023104/5.
- (39) Schmidt, U.; Dieing, T.; Ibach, W.; Hollricher, O. *Microsc. Today* **2011**, *19*, 30–33.
- (40) Domke, K. F.; Pettinger, B. *ChemPhysChem* **2010**, *11*, 1365–1373.
- (41) Hartschuh, A. *Angew. Chem., Int. Ed.* **2008**, *47*, 8178–8191.
- (42) Łojewska, J.; Knapik, A.; Jodłowski, P.; Łojewski, T.; Kolodziej, A. *Catal. Today* **2013**, *216*, 11–17.
- (43) Stiles, P. L.; Dieringer, J. A.; Shah, N. C.; Van Duyne, R. P. *Annu. Rev. Anal. Chem.* **2008**, *1*, 601–626.
- (44) Fleischmann, M.; Hendra, P. J.; McQuillan, A. J. *Chem. Phys. Lett.* **1974**, *26*, 163–166.
- (45) Cialla, D.; Deckert-Gaudig, T.; Budich, C.; Laue, M.; Möller, R.; Naumann, D.; Deckert, V.; Popp, J. *J. Raman Spectrosc.* **2009**, *40*, 240–243.
- (46) Ru, E. L.; Etchegoin, P. *Principles of Surface-Enhanced Raman Spectroscopy and Related Plasmonic Effects*; Elsevier: New York, 2009.
- (47) Hayazawa, N.; Inouye, Y.; Sekkat, Z.; Kawata, S. *Opt. Commun.* **2000**, *183*, 333–336.

- (48) Asthana, B. P.; Deckert, V.; Shukla, M. K.; Kiefer, W. *Chem. Phys. Lett.* **2000**, *326*, 123–128.
- (49) Schmid, T.; Opilik, L.; Blum, C.; Zenobi, R. *Angew. Chem., Int. Ed.* **2013**, *52*, 5940–5954.
- (50) Moskovits, M. *Rev. Mod. Phys.* **1985**, *57*, 783–826.
- (51) Stadler, J.; Schmid, T.; Zenobi, R. *ACS Nano* **2011**, *5*, 8442–8448.
- (52) Pahlow, S.; März, A.; Seise, B.; Hartmann, K.; Freitag, I.; Kämmer, E.; Böhme, R.; Deckert, V.; Weber, K.; Cialla, D.; Popp, J. *Eng. Life Sci.* **2012**, *12*, 131–143.
- (53) Zhang, R.; Zhang, Y.; Dong, Z. C.; Jiang, S.; Zhang, C.; Chen, L. G.; Zhang, L.; Liao, Y.; Aizpurua, J.; Luo, Y.; Yang, J. L.; Hou, J. G. *Nature* **2013**, *498*, 82–86.
- (54) Harrick, N. J. *Internal Reflection Spectroscopy*; John Wiley & Sons, Inc.: New York, 1967.
- (55) Brucherseifer, M.; Kranz, C.; Mizaikoff, B. *Anal. Chem.* **2007**, *79*, 8803–8806.
- (56) Verity, J. E.; Chhabra, N.; Sinnathamby, K.; Yip, C. M. *Biophys. J.* **2009**, *97*, 1225–1231.
- (57) Neubauer, D.; Scharpf, J.; Pasquarelli, A.; Mizaikoff, B.; Kranz, C. *Analyst* **2013**, *138*, 6746–6752.
- (58) Amenabar, I.; Poly, S.; Nuansing, W.; Hubrich, E. H.; Govyadinov, A. A.; Huth, F.; Krutokhvostov, R.; Zhang, L.; Knez, M.; Heberle, J.; Bittner, A. M.; Hillenbrand, R. *Nat. Commun.* **2013**, *4*, 2890–2898.
- (59) Li, J. J.; Yip, C. M. *Biochim. Biophys. Acta* **2013**, *1828*, 2272–2282.
- (60) Hillenbrand, R.; Keilmann, F. *Phys. Rev. Lett.* **2000**, *85*, 3029–3032.
- (61) Huth, F.; Govyadinov, A.; Amarie, S.; Nuansing, W.; Keilmann, F.; Hillenbrand, R. *Nano Lett.* **2012**, *12*, 3973–3978.
- (62) Dazzi, A.; Prazeres, R.; Glotin, F.; Ortega, J. M. *Ultramicroscopy* **2007**, *107*, 1194–1200.
- (63) Rice, J. H. *Nanoscale* **2010**, *2*, 660–667.
- (64) Yeo, B.-S.; Stadler, J.; Schmid, T.; Zenobi, R.; Zhang, W. *Chem. Phys. Lett.* **2009**, *472*, 1–13.
- (65) Schmid, T.; Yeo, B.-S.; Leong, G.; Stadler, J.; Zenobi, R. J. *Raman Spectrosc.* **2009**, *40*, 1392–1399.
- (66) Kranz, C. *Analyst* **2014**, *139*, 336–352.
- (67) Eaton, P. W. *Atomic Force Microscopy*; Oxford University Press: Oxford, U.K., 2010.
- (68) Liu, H.-Y.; Fan, F. R. F.; Lin, C. W.; Bard, A. J. *J. Am. Chem. Soc.* **1986**, *108*, 3838–3839.
- (69) Bard, A. J.; Fan, F. R. F.; Pierce, D. T.; Unwin, P. R.; Wipf, D. O.; Zhou, F. *Science* **1991**, *254*, 68–74.
- (70) Macpherson, J. V.; Unwin, P. R. *Anal. Chem.* **2000**, *72*, 276–285.
- (71) Abbou, J.; Demaille, C.; Druet, M.; Moiroux, J. *Anal. Chem.* **2002**, *74*, 6355–6363.
- (72) Macpherson, J. V.; Jones, C. E.; Barker, A. L.; Unwin, P. R. *Anal. Chem.* **2002**, *74*, 1841–1848.
- (73) Huang, K.; Anne, A.; Bahri, M. A.; Demaille, C. *ACS Nano* **2013**, *7*, 4151–4163.
- (74) Kranz, C.; Friedbacher, G.; Mizaikoff, B.; Lugstein, A.; Smoliner, J.; Bertagnolli, E. *Anal. Chem.* **2001**, *73*, 2491–2500.
- (75) Gullo, M. R.; Frederix, P. L. T. M.; Akiyama, T.; Engel, A.; DeRooij, N. F.; Staufer, U. *Anal. Chem.* **2006**, *78*, 5436–5442.
- (76) Dobson, P. S.; Weaver, J. M. R.; Holder, M. N.; Unwin, P. R.; Macpherson, J. V. *Anal. Chem.* **2005**, *77*, 424–433.
- (77) Eifert, A.; Smirnov, W.; Frittmann, S.; Nebel, C.; Mizaikoff, B.; Kranz, C. *Electrochem. Commun.* **2012**, *25*, 30–34.
- (78) Kueng, A.; Kranz, C.; Lugstein, A.; Bertagnolli, E.; Mizaikoff, B. *Angew. Chem., Int. Ed.* **2005**, *44*, 3419–3422.
- (79) Anne, A.; Cambril, E.; Chovin, A.; Demaille, C.; Goyer, C. *ACS Nano* **2009**, *3*, 2927–2940.
- (80) Ueda, A.; Niwa, O.; Maruyama, K.; Shindo, Y.; Oka, K.; Suzuki, K. *Angew. Chem., Int. Ed.* **2007**, *46*, 8238–8241.
- (81) Janshoff, A.; Galla, H. J.; Steinem, C. *Angew. Chem., Int. Ed.* **2000**, *39*, 4004–4032.
- (82) Sauerbrey, G. *Z. Phys.* **1959**, *155*, 206–222.
- (83) Hayden, O.; Bindeus, R.; Dickert, F. L. *Meas. Sci. Technol.* **2003**, *14*, 1876–1881.
- (84) Johannsmann, D.; Reviakine, I.; Rojas, E.; Gallego, M. *Anal. Chem.* **2008**, *80*, 8891–8899.
- (85) Smith, E. L.; Barron, J. C.; Abbott, A. P.; Ryder, K. S. *Anal. Chem.* **2009**, *81*, 8466–8471.
- (86) Cooks, R. G.; Ouyang, Z.; Takats, Z.; Wiseman, J. M. *Science* **2006**, *311*, 1566–1570.
- (87) Kottke, P. A.; Degertekin, F. L.; Fedorov, A. G. *Anal. Chem.* **2010**, *82*, 19–22.
- (88) Otsuka, Y.; Shide, S.; Naito, J.; Kyogaku, M.; Hashimoto, H.; Arakawa, R. *Rapid Commun. Mass Spectrom.* **2012**, *26*, 2725–2732.
- (89) Ovchinnikova, O. S.; Kjoller, K.; Hurst, G. B.; Pelletier, D. A.; Van Berkel, G. J. *Anal. Chem.* **2014**, *86*, 1083–1090.